Supplemental material for:
Efficient photon detection from color centers in a diamond optical waveguide

I. THEORETICAL ESTIMATE OF THE SIDE-COLLECTION EFFICIENCY

To estimate the expected efficiency of the side-collection technique, we begin by calculating the fraction of NV fluorescence confined within the diamond by total internal reflection (TIR) on first incidence of the emitted photons with the planar diamond chip surface. This fraction depends upon the angle of the emission dipole with respect to the assumed (100) polished surfaces of the diamond chip. We consider the class of NVs with the symmetry axis oriented along the [111] direction, although this calculation is valid for any of the four NV orientations.[1] NV fluorescence is then associated with two orthogonal emission dipoles, D_x and D_y, in the (111) plane[2] [Fig. S1]. The orientation of the dipoles is determined by the direction of non-axial local strain, which varies from location to location within the diamond. We therefore consider the average emission pattern from an ensemble of NVs with orthogonal dipole moments randomly oriented in the (111) plane.

For this calculation, we consider the basis of orthogonal dipoles D_x and D_y oriented in the $[01\bar{1}]$ and $[2\bar{1}\bar{1}]$ directions respectively. The normalized emission intensity distributions of these dipoles, after rotating into spherical coordinates with the zenith in the [100] direction, are then given by:

$$I_{D_x} = \frac{3}{8\pi}\left[1 - \sin^2(\theta)\cos^2(\phi)\right] , \tag{S1}$$

$$I_{D_y} = \frac{3}{8\pi}\left\{1 - \left[\sqrt{\frac{2}{3}}\cos(\theta) - \sqrt{\frac{1}{3}}\sin(\theta)\sin(\phi)\right]^2\right\} \tag{S2}$$

For a dipole with arbitrary orientation in the (111) plane, defined by the angle α [Fig. S1], the normalized emission intensity distribution is

$$I_\alpha = \cos^2(\alpha) I_{D_x} + \sin^2(\alpha) I_{D_y}. \tag{S3}$$

By averaging the two orthogonal dipoles in all possible orientations, we therefore find that the average normalized intensity distribution for NV emission is

$$I_{NV} = \frac{1}{2}\left(I_{D_x} + I_{D_y}\right). \tag{S4}$$

The fraction of NV fluorescence confined by TIR between the (100) surfaces of the diamond is then given by

$$f_{TIR} = \int_{\theta_c}^{\pi-\theta_c}\int_0^{2\pi} I_{NV}\sin(\theta) d\phi d\theta, \tag{S5}$$

where $\theta_c = \arcsin(1/n_d) = 24.6°$ is the critical angle for a diamond-air interface, and $n_d = 2.4$ is the diamond refractive index.

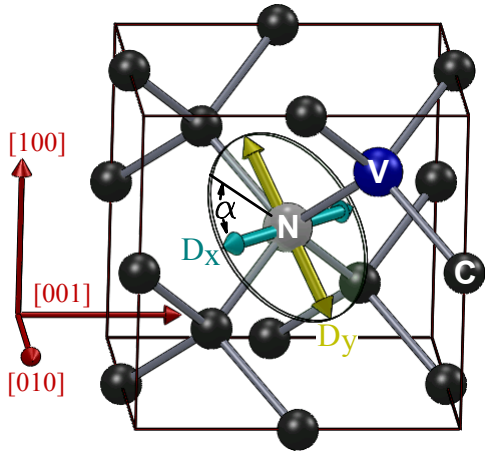

FIG. S1. NV photon emission is associated two orthogonal transition dipole moments, D_x and D_y, in the plane perpendicular to the NV symmetry axis.

From Eq. (S5), we find that on average 91% of the light emitted by NVs suffers TIR on first incidence with the planar diamond chip surfaces, and thus can be guided to the edges of the diamond by TIR. Much of this light can also be confined by TIR off the edges, so we consider this fraction to be an upper bound on side-collection efficiency.

Determining the precise fraction of light that exits the edges of the diamond is a complicated calculation that depends on details such as the diamond shape and the roughness of its surfaces. To approximate the conditions of the experimental demonstration described in this work, we make several simplifying assumptions: (i) light originates in the center of a thin, square diamond chip with perfectly smooth surfaces; (ii) the diamond edges are parallel to the (010) and (001) planes and contact quartz interfaces ($n_q = 1.5$); and (iii) the acceptance angle of the detectors is 56°. We can then estimate a conservative lower bound on the side-collection efficiency by assuming that light reflected off any edge of the diamond is lost. By changing the limits of integration in Eq. (S5) to match theses assumptions, we find that $\sim 29\%$ of the light from NVs reaches the detectors after contact with a single edge. The photon collection efficiency of the side-collection method is therefore expected to be in the range of $29\% < \eta_c < 91\%$ if many diffuse reflections between the edges of the diamond are allowed.

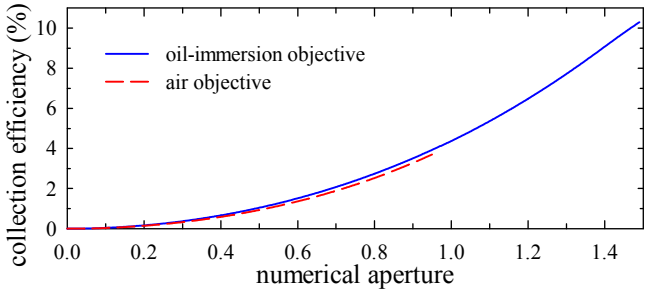

FIG. S2. Calculated collection efficiencies of NV fluorescence by oil-immersion or air microscope objectives through the (100) surface of a diamond chip, as a function of NA.

II. CALCULATING MICROSCOPE OBJECTIVE COLLECTION EFFICIENCIES

A rough estimate of the collection efficiency of a microscope objective can be obtained from the equation

$$\eta_c \simeq \int_0^{\theta_{max}} \int_0^{2\pi} I_{\mathrm{NV}} \sin(\theta) d\phi d\theta, \tag{S6}$$

where $\theta_{max} = \arcsin(\mathrm{NA}/\mathrm{n_d})$ and NA is the numerical aperture of the objective. However, this equation does not take into account reflection at the diamond chip interface, which is on the order of 17% or 5% for a diamond-air or diamond-oil interface, respectively, at near-normal angles of incidence. For a more accurate calculation of the collection efficiency, we must consider the s-polarized and p-polarized portions of the NV emission pattern separately.

We find that the s-polarized and p-polarized portions of the intensity distributions given in Eqs. (S1,S2) are

$$I_{\mathrm{D_{x,s}}} = \frac{3}{8\pi} \sin^2(\theta) \sin^2(\phi) \ , \tag{S7}$$

$$I_{\mathrm{D_{x,p}}} = \frac{3}{8\pi} \cos^2(\theta) \ , \tag{S8}$$

$$I_{\mathrm{D_{y,s}}} = \frac{1}{8\pi} \sin^2(\theta) \cos^2(\phi) \ , \text{ and} \tag{S9}$$

$$I_{\mathrm{D_{y,p}}} = \frac{1}{8\pi} \left[1 + \sqrt{2} \sin(2\theta) \sin(\phi) + \sin^2(\theta)\right] . \tag{S10}$$

The average NV emission profiles for s-polarized and p-polarized light are then

$$I_{\mathrm{NV_s}} = \frac{1}{2} \left(I_{\mathrm{D_{x,s}}} + I_{\mathrm{D_{y,s}}}\right) \ , \tag{S11}$$

$$I_{\mathrm{NV_p}} = \frac{1}{2} \left(I_{\mathrm{D_{x,p}}} + I_{\mathrm{D_{y,p}}}\right) . \tag{S12}$$

The collection efficiency of a microscope objective is then given by

$$\eta_c = \int_0^{\theta_{max}} \int_0^{2\pi} \left[I_{\mathrm{NV_s}} T_s(\theta) + I_{\mathrm{NV_p}} T_p(\theta)\right] \sin(\theta) d\phi d\theta, \tag{S13}$$

where T_s and T_p are the transmission coefficients of s-polarized and p-polarized light through the interface, as given by the Fresnel equations. The objective collection efficiencies calculated from Eq. (S13) are plotted in Fig. S2 as a function of NA. This formula was also used to calculate the objective collection efficiencies given in the main body of this paper.

III. EXPERIMENTAL METHODS USED FOR AC MAGNETOMETRY

A. Application and Alignment of a Static Magnetic Field

At zero magnetic field, the NV spin is quantized along the NV symmetry axis, and the $|\mathrm{m_s} = 0>$ and $|\mathrm{m_s} = \pm 1>$ ground states are split by 2.87 GHz. When a small magnetic field ($\ll 500$ G) is applied, the $|\mathrm{m_s} = 0> \leftrightarrow |\mathrm{m_s} = \pm 1>$ spin transition frequencies split due to the Zeeman effect by an amount that is approximately proportional to the projection of the magnetic field along the NV symmetry axis. For the experiments depicted in Fig. 3 of the main text, a 37.5 G static magnetic field was aligned along the [111] direction using a permanent magnet mounted on a tip-tilt stage. This allowed us to selectively drive the $|\mathrm{m_s} = 0> \leftrightarrow |\mathrm{m_s} = +1>$ spin transition of [111]-oriented NVs, while having all other spin transition frequencies detuned by at least 65 MHz.

We note that to obtain an optimal $\mathrm{T_2}$ coherence for a diamond sample containing a natural isotopic abundance of ^{13}C, it is important to first precisely align the magnetic field along the NV symmetry axis.[3] To do this, we measured the resonance frequencies of the $|\mathrm{m_s} = 0> \leftrightarrow |\mathrm{m_s} = \pm 1>$ spin transitions for NVs oriented along the $[1\bar{1}\bar{1}]$, $[\bar{1}1\bar{1}]$, and $[\bar{1}\bar{1}1]$ directions by using continuous wave (CW) laser excitation and microwave driving, and observing the dips in the fluorescence signal as the microwave frequency is tuned on resonance.[4] We then adjusting the angle of the permanent magnet using the tip-tilt stage until the transition frequencies for the three different NV orientations overlapped (because the magnitude of the projection of a [111]-oriented field on these three crystallographic directions is the same).

B. Resonant Driving of NV Spin Transitions Using Microwave Fields

For the experiments depicted in Fig. 3 of the main text, the $|\mathrm{m_s} = 0> \leftrightarrow |\mathrm{m_s} = 1>$ spin transitions of [111]-oriented NVs in the diamond chip were driven with a 2.975 GHz microwave field. A signal generator (Agilent E4428C) produced a CW output at 2.975 GHz, which was converted to short pulses of chosen duration using a fast TTL-driven switch (Mini-Circuits ZASWA-2-50DR+). The power of the pulsed microwave signal from the switch were amplified to 10 W using a pair of ampli-

fiers in series (Mini-Circuits ZHL-42 output to an Ophir 5803025). This amplified signal was then applied across a 1.5 mm diameter loop of wire near the (100) polished surface of the diamond. The laser beam used to excite the NV centers passed through the center of this loop, so that the measurement volume was in a region where there was an approximately uniform oscillating magnetic field in the [100] direction.

The Rabi oscillation frequency between the $|m_s = 0>$ and $|m_s = 1>$ states in this configuration was ≈ 12.5 MHz. Spatial variation of the microwave Rabi frequency within the laser excitation volume led to a decay in the Rabi curve, and also to an imperfect 2π rotation of the NV spin ensemble at the end of the spin echo sequence depicted in Fig. 3(a), resulting in a 2% reduction in the signal for $\tau = 0$ in Fig. 3(b). This spin rotation error could be corrected in the future by applying a more uniform microwave field, for example by using a Helmholtz coil configuration. This is a topic that will be investigated in future experiments for improved measurement contrast and magnetometer sensitivity.

For the magnetometry measurements depicted in Fig. 3(c), the phase of the final $\pi/2$ microwave pulse in the spin echo sequence depicted in Fig. 3(a) was shifted by 90° with respect to the first two pulses of the sequence. This shifted the phase of the AC magnetometry curve by 90°, so that the maximum slope in the AC magnetometry curve, and therefore maximum magnetic field sensitivity, occurs for zero applied AC magnetic field. This phase shift was accomplished using an IQ mixer (Marki Microwave IQ1545LMP) placed between the signal generator and switch.

C. Optical NV Spin Polarization and Measurement

The NV spin state was measured and initialized using light from a CW 532 nm laser (Coherent Verdi G7), which could be rapidly switched on and off to produce pulses of light using an acousto-optic modulator (Isomet M1133-aQ80L-1.5). For the AC magnetometry measurements described in the main text, the objective in Fig. 2(a) of the main text was replaced by a lens with a focal length of 25.4 mm. We used a CMOS camera (Thorlabs DCC1545M) to directly measure the Gaussian beam intensity profile, and found that the $1/e^2$ width of the Gaussian beam at the focus was ≈ 25 μm. The center of the diamond chip was then precisely placed at the beam focal position using a translation stage. The beam diameter was approximately constant across the 0.2 mm thickness of the diamond chip, so we can estimate that the laser excitation volume within the diamond chip was $\approx 10^{-4}$ mm^3. We estimate that the diamond chip had a uniform NV-density $\sim 10^{15}$ cm^{-3}, and therefore that the number of NV centers probed by the laser beam was $\sim 10^8$. For the magnetometry measurements described in the main text, the laser power was set to 670 mW. This corresponds to an average laser intensity of 140 kW/cm^2 within the laser excitation volume.

At the end of the spin-echo sequence depicted in Fig. 3(a) of the main text, the NV spin state was measured using a 300 ns duration "readout" laser pulse. This was followed 6 μs later by a 300 ns duration "pump" laser pulse. The combined 600 ns of laser excitation time was sufficient to initialize the NV spin in the $|m_s = 0>$ state at the start of the subsequent spin-echo measurement sequence. The 6 μs delay between the two pulses allowed us to independently measure the integrated fluorescence signal from the charge amplifier (Cremat Inc. CR-112) corresponding to either pulse using a data acquisition (DAQ) card (National Instruments PCI-MIO-16E-4). The duration of the "readout" laser pulse was independently varied to maximize the sensitivity of the magnetometry measurement, and we found that a 300 ns duration pulse was optimal. The total duration of a single magnetometry measurement [see Fig. 3(c) in the main text] was therefore 57 μs, 50 μs spent sensing the applied AC magnetic field during the microwave spin-echo pulse sequence, and 7 μs spent measuring the NV spin state and initializing the NV spin for the subsequent measurement. This measurement sequence was repeated continuously.

D. Measurement Noise

The fluorescence signal recorded during the "readout" laser pulse was normalized with respect to the excitation laser intensity, in order to reduce noise caused by fluctuations in the laser intensity. We evaluated the noise in the resulting normalized data set, and found that it was nearly identical to the noise level recorded when we performed the measurements with the laser and microwave field turned off. We therefore concluded that the noise in our magnetometry measurements were dominated almost exclusively by the electronic noise in the fluorescence measurement circuitry (four photodiodes connected to a charge amplifier, read out with a DAQ card). This noise level was approximately ten times larger than the specified noise level for the combined charge amplifier and DAQ card, and we believe that this was largely due to the large parasitic capacitance and leakage current of the photodiodes used for the experiment (Advanced Photonix PDB-C609-2). By switching to photodiodes with better properties and improving the design of the readout electronics from this initial prototype device, we expect that future measurements will not be limited by electronic noise in this manner.

IV. BIBLIOGRAPHY

[1]The four possible NV orientations ([111], [1$\bar{1}\bar{1}$], [$\bar{1}$1$\bar{1}$], and [$\bar{1}\bar{1}$1]) all have the same angle with respect to the (100) surface.

[2]R. J. Epstein, F. M. Mendoza, Y. K. Kato, and D. D. Awschalom, Nat. Phys. **1**, 94 (2005).

[3] P. L. Stanwix, L. M. Pham, J. R. Maze, D. Le Sage, T. K. Yeung, P. Cappellaro, P. R. Hemmer, A. Yacoby, M. D. Lukin, and R. L. Walsworth, Phys. Rev. B **82**, 201201 (2010).
[4] A. Gruber, A. Dräbenstedt, C. Tietz, L. Fleury, J. Wrachtrup, and C. v. Borczyskowski, Science **276**, 2012 (1997).